

# End of multi-field inflation and the perturbation spectrum

Jinn-Ouk Gong\*

*International Center for Astrophysics  
Korea Astronomy and Space Science Institute  
Daejeon, Republic of Korea*

December 2, 2024

## Abstract

We investigate the dynamics of inflation models driven by multiple, decoupled scalar fields and calculate the Hubble parameter and the amplitude of the lightest field at the end of inflation which may be responsible for interesting, or possibly dangerous cosmological consequences after inflation. The results are very simple and similar to those of the single field inflation, mainly depend on the underlying spectrum of the masses. The mass distribution is heavily constrained by the power spectrum of density perturbations  $\mathcal{P}$  and the spectral index  $n_s$ . The overall mass scale gives the amplitude of  $\mathcal{P}$  and  $n_s$  is affected by the number of fields and the spacing between masses in the distribution. The drop-out effect of the massive fields makes the perturbation spectrum typically redder than the single field inflation spectrum. We illustrate this using two different mass distributions.

---

\*jgong@kasi.re.kr

# 1 Introduction

After its advent, inflation [1] has been very successful to solve many cosmological problems of the standard hot big bang cosmology and its predictions are consistent with the recent observations [2, 3]: inflation can explain the homogeneity, isotropy and flatness of the observable universe, as well as the origin of the large scale structure in the universe. Interestingly, the simplest possibility, i.e. the model of chaotic inflation with quadratic potential  $V(\phi) = m^2\phi^2/2$  is still consistent with the WMAP three year results [3]. Thus it is natural to try to build such a fully realistic inflationary scenario in the context of string theory, the most promising candidate of the fundamental theory of nature. However, it is still unclear how to find successful inflationary scenarios in string theory. Especially, if the vacuum expectation value of the inflaton field  $\phi$  is beyond the Planck scale  $m_{\text{Pl}}$ , which is the case for the simplest  $m^2\phi^2$  chaotic inflation, generally large radiative corrections are expected and they would modify the inflaton potential  $V(\phi)$  and the predictions based on the original form of the effective potential will be no more reliable.

Fortunately, after the de Sitter vacua construction in type IIB theory [4], there have been considerable advances to this end for recent years [5]. An interesting scenario named N-flation was recently proposed [6] where the  $m^2\phi^2$  inflation model is achieved by the assisted inflation mechanism [7]: many ( $N \gg 1$ ) fields combine to drive inflation with the displacements being less than  $m_{\text{Pl}}$ . These fields are considered to be the string axion fields, which are known to exist abundantly in string theory, and they have flat potentials even after all the moduli are stabilised. In Ref. [6] the special case where all the masses are the same is highlighted, and subsequently more general extensions were investigated in Refs. [8, 9]. The general and qualitative evolution of the fields is however clear: the most massive fields roll down their potentials to the minima, and the light fields are responsible for the later inflationary stages. Here one important thing is that, at the end of inflation, *not* all the fields are relaxed to the minima. For the single field inflation with  $V(\phi) = m^2\phi^2/2$ , as we will see in the next section, inflation ends well before  $\phi$  reaches the minimum of the potential. Likewise, inflation proceeds no more although there are still some fields whose amplitudes are non-zero. These non-zero fields are of cosmological importance after inflation: they may lead to interesting, or possibly dangerous cosmological consequences. For example, they may oscillate and decay into dark matter particles [10], they can produce additional perturbations via curvaton mechanism<sup>1</sup> [12], and they would be responsible for the preheating [13] of the universe after inflation. They can, of course, produce gravitino at an unacceptable level [14], spoiling the successful predictions of the big bang nucleosynthesis [15]. The dynamics of the fields depends on the underlying spectrum of masses, which is revealed via the power spectrum  $\mathcal{P}$  and the spectral index  $n_s$ : they depend on the detail of the mass distribution.

Our purpose in this paper is to study the dynamics of this class of multiple field inflation to calculate several interesting physical quantities at the end of inflationary regime in connection with the power spectrum  $\mathcal{P}$  and the spectral index  $n_s$ . Since the lightest field keeps the largest amplitude at the end of inflation, we will mainly focus on this field and its mass: also we can describe the evolution of the lightest field under slow-roll approximation, and this helps to simplify the calculations. This paper is outlined as follows. In Section 2, we first briefly review the simplest chaotic inflation model with  $V(\phi) = m^2\phi^2/2$  and calculate some quantities of the

---

<sup>1</sup>Note that for the curvaton mechanism to work properly, we must put more constraints on the parameter space of the model under consideration [11] in addition to the conditions for successful inflationary phase.

model. In Section 3, we calculate the Hubble parameter, the number of fields with non-zero amplitudes and the amplitude of the lightest field at the end of inflation. In Section 4 we apply the results of the previous section to two interesting mass distributions, and compare with the single field inflation case. In Section 5 we summarise and conclude.

## 2 Single field inflation

In this section, we recall the inflation model where accelerated expansion is driven by a single inflaton field with simple quadratic potential [1]. The inflaton potential is given by

$$V(\phi) = \frac{1}{2}m^2\phi^2, \quad (1)$$

and with the slow-roll equation of motion for  $\phi$ ,

$$3H\dot{\phi} + m^2\phi = 0, \quad (2)$$

the total number of  $e$ -folds is

$$\mathcal{N} = \int Hdt \simeq \frac{\phi_i^2}{4m_{\text{Pl}}^2}. \quad (3)$$

Then, to obtain  $\mathcal{N} \gtrsim 60$ , we need  $\phi_i \gtrsim 4\sqrt{15}m_{\text{Pl}} \sim 15m_{\text{Pl}}$ : the initial value of the inflaton  $\phi$  is required to be much larger than  $m_{\text{Pl}}$ . Now, from the acceleration equation

$$\begin{aligned} \frac{\ddot{a}}{a} &= \frac{-1}{6m_{\text{Pl}}^2}(\rho + 3p) \\ &= \frac{V(\phi) - \dot{\phi}^2}{3m_{\text{Pl}}^2}, \end{aligned} \quad (4)$$

we find that inflation ends when

$$\dot{\phi}^2 \geq \frac{1}{2}m^2\phi^2, \quad (5)$$

i.e. the kinetic energy of the field becomes greater than half of the potential energy. Using Eq. (2) to eliminate  $\dot{\phi}$ , the value of the Hubble parameter at the end of inflation is estimated as

$$H_{\text{end}} = \frac{\sqrt{2}}{3}m. \quad (6)$$

Note that Eq. (5) is equivalent to the condition that the slow-roll parameter

$$\epsilon = -\frac{\dot{H}}{H^2} = \frac{1}{2m_{\text{Pl}}^2} \left( \frac{\dot{\phi}}{H} \right)^2 \quad (7)$$

becomes larger than 1. Substituting Eq. (6) into Eq. (7) and using Eq. (5), we find that at the end of inflation  $\phi$  has the amplitude

$$\phi_{\text{end}} = \frac{2\sqrt{2}}{3}m_{\text{Pl}}. \quad (8)$$

The mass of the inflaton field is heavily constrained by the amplitude of the primordial density perturbations<sup>2</sup>. The leading-order<sup>3</sup> power spectrum of primordial density perturbations is given by [1]

$$\mathcal{P} = \frac{m^2 \phi^4}{96\pi^2 m_{\text{Pl}}^6}, \quad (9)$$

and the corresponding spectral index by

$$n_s - 1 = -\frac{8m_{\text{Pl}}^2}{\phi^2}. \quad (10)$$

Using the COBE observation  $\delta_H = 2\sqrt{\mathcal{P}}/5 \simeq 1.91 \times 10^{-5}$ , we find

$$m \simeq 6.07 \times 10^{-6} m_{\text{Pl}}. \quad (11)$$

Note that  $n_s$  is independent of  $m$  and is given by  $n_s \simeq 0.967$  when  $\phi = 4\sqrt{15}m_{\text{Pl}}$ , i.e. 60  $e$ -folds before the end of inflation<sup>4</sup>. In Fig. 1, we illustrate some results of numerical calculations, and in Table 2 we compare the corresponding analytic and numerical estimates.

	$\mathcal{N}$	$\phi_{\text{end}}$	$\phi_{\text{COBE}}$	$H_{\text{end}}$	$\mathcal{P}$	$n_s$
analytic	100.00	0.942809	15.4919	$0.471405 \times 10^{-5}$	$6.18101 \times 10^{-9}$	0.966942
numerical	100.97	1.00934	15.4209	$0.574670 \times 10^{-5}$	$5.96853 \times 10^{-9}$	0.966359

Table 1: Analytic and numerical estimates of several important quantities of the calculations of Fig. 1.  $\phi_{\text{end}}$ ,  $\phi_{\text{COBE}}$  and  $H_{\text{end}}$  are written in the unit of  $m_{\text{Pl}}$ . We set the COBE point to be 60  $e$ -folds before inflation ends, and  $\mathcal{P}$  and  $n_s$  are estimated at that point. Generally the analytic results agree with the corresponding numerical ones.

### 3 Multiple field case

Now let us consider the inflation case with multiple, uncoupled fields [6]. Here inflation is driven by a number of non-interacting string axion fields. If each axion field is displaced not too far from the minimum, we can write the potential as

$$V = \sum_{i=1}^N \frac{1}{2} m_i^2 \phi_i^2, \quad (12)$$

---

<sup>2</sup>Note that the inflationary energy scale is constrained from the detailed calculations on the amplitude of the power spectrum of the primordial gravitational waves [16].

<sup>3</sup>For the calculations with higher-order corrections in the slow-roll parameters, see e.g. [17].

<sup>4</sup>Note that, in fact, there exist some level of uncertainty on exactly when the observable large scale perturbations were generated. While for most models of inflation the corresponding  $e$ -folds lies between 50 and 60 [18], the values of  $\mathcal{P}$  and especially  $n_s$  are similar: we have  $n_s = 0.963280$  and  $0.959581$  for 55 and 50  $e$ -folds before the end of inflation, respectively. Thus, in this paper we keep evaluating  $\mathcal{P}$  and  $n_s$  before 60  $e$ -folds.

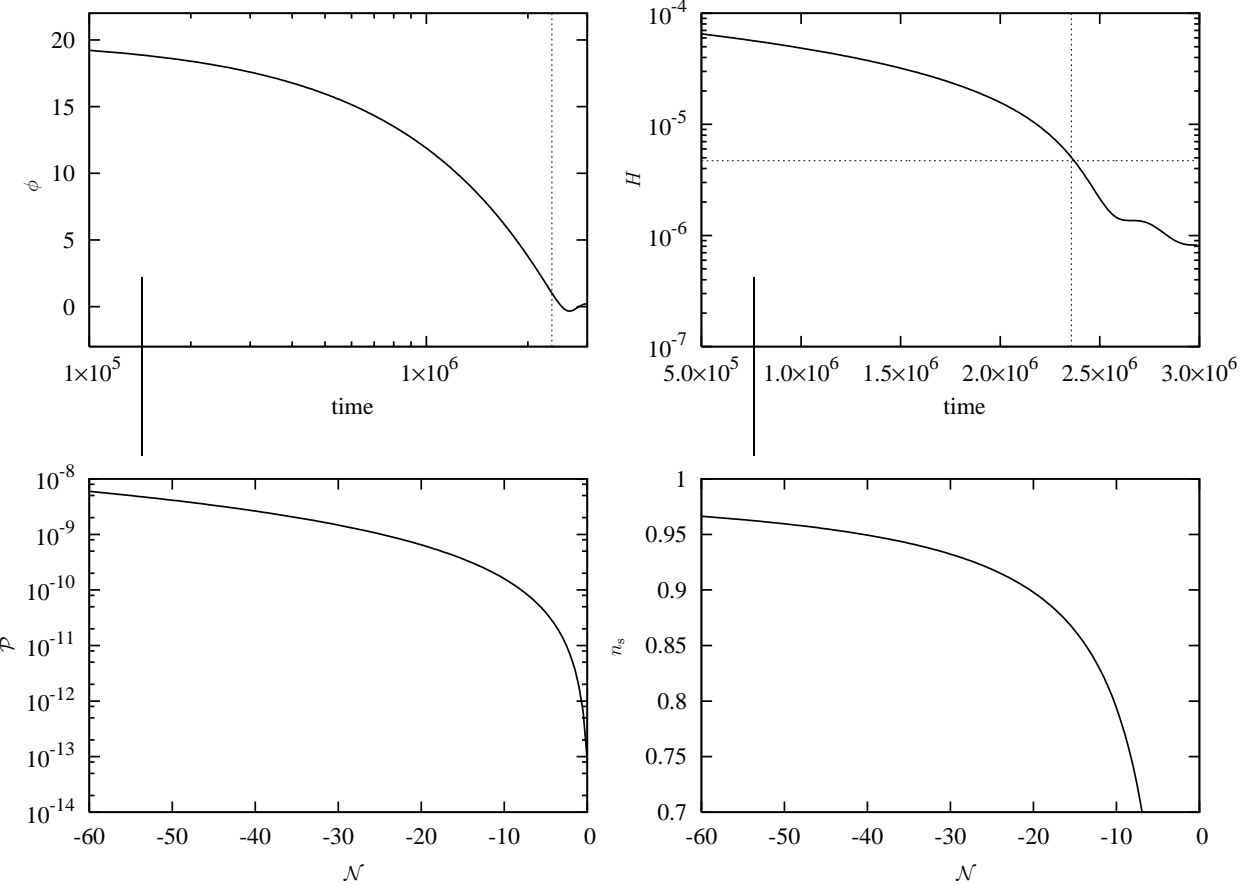


Figure 1: Numerical results of the single field inflation with the initial amplitude  $\phi_i = 20m_{\text{Pl}}$  and the mass  $m = 10^{-5}m_{\text{Pl}}$ . The dotted lines indicate the end of inflation: in the plot of  $H$  (upper right) the horizontal dotted line is  $H_{\text{end}}$ , given by Eq. (6). In the lower row, we set  $\mathcal{N} = 0$  as the end of inflation.

where we assume that there are  $N$  axion fields. The total number of  $e$ -folds is then given by

$$\mathcal{N} = \frac{\sum_i \phi_i^{(0)2}}{4m_{\text{Pl}}^2}, \quad (13)$$

where  $\phi_i^{(0)}$  is the initial value of  $\phi_i$ . From Eq. (4), we obtain

$$\frac{\ddot{a}}{a} = \frac{1}{3m_{\text{Pl}}^2} \sum_{i=1}^N \left( \frac{1}{2} m_i^2 \phi_i^2 - \dot{\phi}_i^2 \right), \quad (14)$$

thus inflation ends when

$$\sum_{i=1}^N \dot{\phi}_i^2 \geq \sum_{i=1}^N \frac{1}{2} m_i^2 \phi_i^2. \quad (15)$$

Now, using the slow-roll equation of motion for  $\phi_i$ ,

$$3H\dot{\phi}_i + m_i^2 \phi_i = 0, \quad (16)$$

we can find that under the slow-roll approximation different fields  $\phi_i$  and  $\phi_j$  satisfy the relation [19]

$$\frac{\dot{\phi}_i}{\dot{\phi}_j} = \frac{m_i^2 \phi_i}{m_j^2 \phi_j}, \quad (17)$$

thus we obtain

$$\left( \frac{\phi_i}{\phi_i^{(0)}} \right)^{1/m_i^2} = \left( \frac{\phi_j}{\phi_j^{(0)}} \right)^{1/m_j^2}. \quad (18)$$

Therefore, we can write  $\phi_i$  and  $\dot{\phi}_i$  in terms of the lightest field  $\phi_N$  and  $\dot{\phi}_N$  as

$$\begin{aligned} \phi_i &= \left( \frac{\phi_N}{\phi_N^{(0)}} \right)^{m_i^2/m_N^2} \phi_i^{(0)}, \\ \dot{\phi}_i &= \frac{m_i^2}{m_N^2} \left( \frac{\phi_N}{\phi_N^{(0)}} \right)^{m_i^2/m_N^2-1} \left( \frac{\phi_i^{(0)}}{\phi_N^{(0)}} \right) \dot{\phi}_N, \end{aligned} \quad (19)$$

respectively. Substituting Eq. (19) into Eq. (15) and using the slow-roll equation of motion for  $\phi_N$ , we find that inflation ends when

$$H_{\text{end}}^2 = \frac{2}{9} \frac{\sum_{i=1}^N m_i^4 \left( \phi_N^{\text{end}} / \phi_N^{(0)} \right)^{2m_i^2/m_N^2}}{\sum_{i=1}^N m_i^2 \left( \phi_N^{\text{end}} / \phi_N^{(0)} \right)^{2m_i^2/m_N^2}}. \quad (20)$$

Because  $\phi_N^{\text{end}} / \phi_N^{(0)} < 1$  at the end of inflation and  $m_i > m_N$  always, the last term of each sum gives the most significant contribution for that sum. Therefore, the Hubble parameter at the end of inflation is

$$H_{\text{end}} \simeq \frac{\sqrt{2}}{3} m_N, \quad (21)$$

where  $m_N$  is the mass of the lightest field. Interestingly, this is exactly the same form as the single field inflation case, Eq. (6). Note that at this point, combining Eq. (21) and the slow-roll equation of  $\phi_N$ , the kinetic energy of the field  $\phi_N$  is half of the potential energy,

$$K_N = \frac{1}{2} V_N, \quad (22)$$

as the case of the single field inflation. Likewise for  $\phi_i$  we can derive a similar relation

$$K_i = \frac{m_i^2}{2m_N^2} V_i. \quad (23)$$

Now, assuming that total  $n$  light fields ( $n < N$ ) contribute at the end of inflation, we write

$$\begin{aligned} H_{\text{end}}^2 &\simeq \frac{2}{9} m_N^2 \\ &= \frac{1}{3m_{\text{Pl}}^2} [(K_{N-n+1} + V_{N-n+1}) + \cdots + (K_N + V_N)]. \end{aligned} \quad (24)$$

As can be seen from Eq. (23), as the mass becomes heavier, the kinetic energy is increasing while the potential energy is decreasing. Thus, we can assume that the energy contribution of each field roughly coincides. Then, Eq. (24) becomes

$$H_{\text{end}}^2 \sim \frac{n}{3m_{\text{Pl}}^2} (K_N + V_N), \quad (25)$$

hence using Eq. (22) the amplitude of the lightest field  $\phi_N$  at the end of inflation is given by

$$\phi_N^{\text{end}} \sim \frac{2\sqrt{2}}{3} \frac{m_{\text{Pl}}}{\sqrt{n}}, \quad (26)$$

which is again similar to the single field case, Eq. (8), divided by some numerical factor  $n$ . Note that this number would be proportional to the total number of fields  $N$  unless the masses are anomalously distributed<sup>5</sup>, hence  $\phi_N^{\text{end}}$  decreases as  $N$  increases: with larger number of fields, the inflationary phase lasts longer until  $\phi_N$  reaches smaller value. To estimate the mass of the most massive field which contributes at the end of inflation, first we observe that heavy fields drop out at the early stages of inflation while light fields drive inflation at late stages. Hence, it is reasonable to assume that the fields which are responsible for the inflation of the last  $e$ -folds have masses within far less than an order of magnitude, otherwise some of them would have already quitted the inflationary regime. Thus, we can set the mass of the heaviest field to be

$$m_{N-n+1} \sim \sqrt{2}m_N. \quad (27)$$

This number  $n$  is dependent on the specific mass distribution as we will see in the next section. We cannot, however, follow the same steps to calculate the power spectrum of curvature perturbations<sup>6</sup> and the spectral index: following  $\delta\mathcal{N}$  formalism [22], they are written as [8, 9]

$$\mathcal{P} = \frac{\sum_i m_i^2 \phi_i^2}{96\pi^2 m_{\text{Pl}}^6} \sum_j \phi_j^2 \quad (28)$$

and

$$n_s - 1 = -4m_{\text{Pl}}^2 \left[ \frac{\sum_i m_i^4 \phi_i^2}{\left( \sum_j m_j^2 \phi_j^2 \right)^2} + \frac{1}{\sum_k \phi_k^2} \right], \quad (29)$$

respectively. From Eq. (29), we can see that the spectrum is *always* redder than the spectrum of the single field inflation<sup>7</sup>. At the end of inflation, the amplitude of  $\phi_N$  has significantly decreased from its initial value  $\phi_N^{(0)}$ , and thus we could ignore all the contributions except the one by  $\phi_N$  in Eq. (20). But before 60  $e$ -folds where the COBE observation is made,  $\phi_N$  is almost frozen and hence the contributions other than  $\phi_N$  should be taken into account.

---

<sup>5</sup>If the axion decay constant could be made far larger than  $m_{\text{Pl}}$ , we can obtain consistent inflationary scenario with very limited number of fields, e.g. only two fields [20].

<sup>6</sup>Generally, it is expected that orthogonal isocurvature perturbations are also generated. See, e.g. [21] for a review.

<sup>7</sup>Note that this is true not only for the quadratic potential given by Eq. (12), but for a set of general power law potentials [23].

## 4 Mass distributions

In this section we illustrate the results of the previous section using two different mass distributions of the axion fields. Here we take  $\phi_1^{(0)} = \dots = \phi_N^{(0)} = m_{\text{Pl}}$  for numerical calculations: when building inflationary models with masses being given by the underlying physics, the one with the largest possible number of  $e$ -folds is favoured because it occupies the greatest volume in the context of eternally inflating universe [24] and is preferred a posteriori. This is implemented by assigning the maximum initial displacement to the fields with a given spectrum of masses.

### 4.1 Exponential distribution

We first consider the exponential mass spectrum where the fields are distributed uniform on logarithmic scale [6, 9],

$$m_i^2 = m_1^2 e^{-(i-1)/\sigma}, \quad (30)$$

where  $i = 1, \dots, N$  is the index of the fields, and  $\sigma$  is the density of fields per logarithmic interval.  $\sigma$  is determined once we decide the heaviest mass  $m_1$ , the lightest mass  $m_N$  and the number of fields  $N$ .

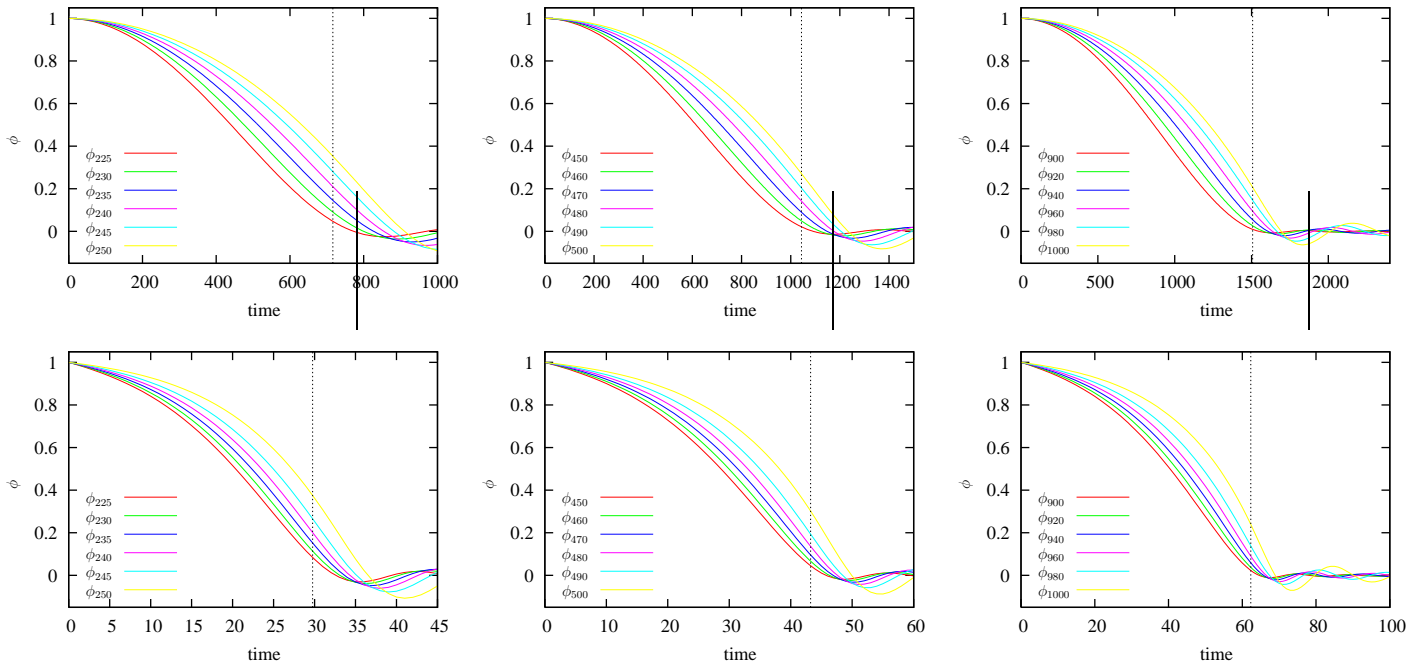


Figure 2: The evolution of the fields. In the upper row, masses are distributed according to Eq. (30) where the most massive mass  $m_1 = m_{\text{Pl}}$ , while in the lower row Eq. (32) is applied with the average mass  $\bar{m} = m_{\text{Pl}}$  and the parameter  $\beta = 1/2$ . We set  $N = 250, 500$  and  $1000$  in the left, middle and right panel, respectively. As in Fig. 1, the vertical dotted line denotes the end of inflation.

We have performed numerical calculations under this mass distribution with the lightest mass being  $1/100$  of the heaviest mass, i.e.  $m_N = 10^{-2}m_1$ . We have tried  $N = 250, 500$  and  $1000$ , with  $m_1 = m_{\text{Pl}}, 10^{-2}m_{\text{Pl}}, 10^{-4}m_{\text{Pl}}$  and  $10^{-6}m_{\text{Pl}}$  for each case. The evolution of several

light fields are shown in the upper row of Fig. 2. Here, we show only the cases where we have set  $m_1 = m_{\text{Pl}}$ , since for other cases the fields follow exactly the same evolutions except for time scale: e.g. it takes  $10^2$  times longer when  $m_1$  becomes  $10^{-2}$  times lighter. The dotted line indicates the end of inflation. As can be seen, heavy fields drop out of the inflationary regime at early times and only a limited number of light fields keep non-zero amplitudes at the end of inflation. To estimate the number of the fields which contribute at the end of inflation, we can combine Eqs. (27) and (30) to obtain

$$n \sim 1 + \frac{(N-1) \log 2}{4 \log 10}, \quad (31)$$

which gives  $n = 19, 38$  and  $76$  for  $N = 250, 500$  and  $1000$ , respectively. Also note that because of the relatively large  $H$ , many fields undergo dissipation [6] at the early stage of inflation, and do not oscillate near the minima.

In the upper row of Fig. 3 we show the power spectrum  $\mathcal{P}$  given by Eq. (28) for each case. Now, we obtain different spectra for different cases: the mass gives overall amplitude, and the number of fields controls the shape of the spectrum. As can be read from Eq. (28), the amplitude of the spectrum is proportional to the sum of the mass squared of every field. We can also understand the reason why the spectrum becomes flatter with larger number of fields as follows: since here we take  $\phi_i^{(i)} = m_{\text{Pl}}$  for all  $i$ , massive fields dominate the total energy density at early times. Therefore as these fields are completely dropping out of the inflationary regime, the Hubble parameter  $H$  is decreasing steeply, making the amplitude  $\mathcal{P}$  decline quickly. This “drop-out” effect of heavy fields weakens when there are many other light fields so the contributions by these fields keep the energy density and hence  $H$  smoothly varying within the slow-roll regime. This is independent of the overall mass scale but dependent only on the number of fields and the spacing between masses. Thus, all in all, we can observe the same shape of the spectrum with the same number of fields.

Now we turn to the spectral index  $n_s$ . As we have discussed above, here  $n_s$  is independent of the overall mass scale, so in the left panel of Fig. 4 we show different indices on different  $N$  only. As anticipated from the discussion above, we obtain larger tilt with smaller number of fields. One interesting thing is the initial steep decrease of the index for  $N = 250$ . This is due to the drop-out effect we discussed above: massive fields which occupy a large fraction of the energy density drop out of the inflationary regime, so  $H$ , and consequently  $\mathcal{P}$  is decreasing quickly. However, soon the contributions by lighter fields under the slow-roll evolution become dominant and there is no more rapid change in  $H$ , so  $\mathcal{P}$  becomes flatter afterwards. Therefore, because of this drop-out effect, typically the spectrum is redder than the spectrum of the single field inflation where such an effect cannot happen.

## 4.2 Marčenko-Pastur law

The mass of string axion depends on the details of the compactification which involves many factors not yet (or formidable to be) computed. Nevertheless, in spite of the unclear microscopic physics, the mass distribution is known to follow the Marčenko-Pastur law [8]: the probability

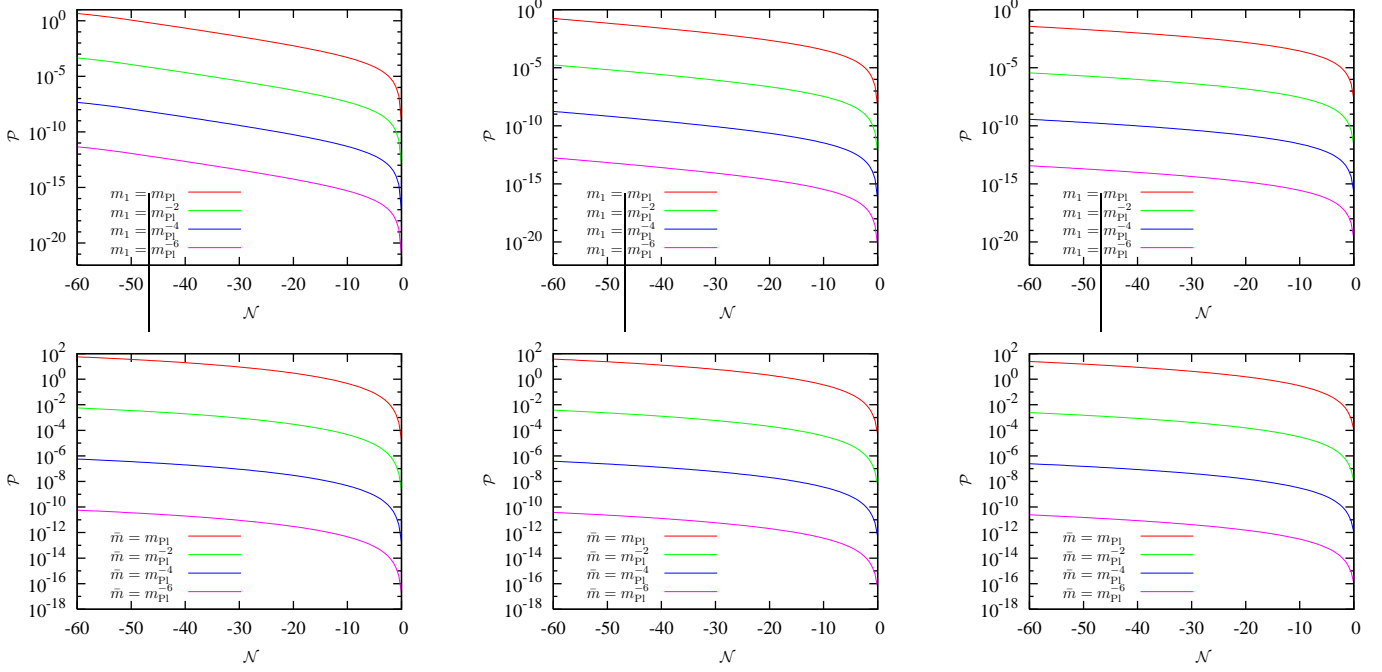


Figure 3: Plots of the power spectra  $\mathcal{P}$  calculated by Eq. (28) corresponding to the calculations in Fig. 2. We follow the mass distribution given by Eqs. (30) and (32) in the upper and lower row, respectively.

density function for  $m^2$  is given by

$$p(m^2) = \frac{\sqrt{\left[\bar{m}^2 (1 + \sqrt{\beta})^2 - m^2\right] \left[m^2 - \bar{m}^2 (1 - \sqrt{\beta})^2\right]}}{2\pi\beta\bar{m}^2 m^2}, \quad (32)$$

where  $\bar{m}$  is the average value of the mass, i.e.  $\langle m^2 \rangle = \bar{m}^2$ , and  $\beta$  is a model dependent parameter whose favourable value is expected to be  $1/2$ . Note that for this case masses are more densely packed than the exponential distribution we have used in the previous section: we have

$$\begin{aligned} m_1 &= 1.707110\bar{m}, \\ m_N &= 0.292893\bar{m} \end{aligned} \quad (33)$$

for  $\beta = 1/2$ .

The evolution of fields according to the Marčenko-Pastur law given by Eq. (32) is shown in the lower row of Fig. 2. Since masses are densely packed, the fields are evolving faster than those under the distribution Eq. (30) we have used in the previous section, where the masses spread over two orders of magnitude. The qualitative evolution of the fields is, however, not too different: heavy fields exit the inflationary regime at early times, and light fields drive inflation at late stages.

The relative dense packing of the masses is easily read from the power spectrum  $\mathcal{P}$  and the spectral index  $n_s$ , which are shown in the lower row of Fig. 3 and in the right panel of Fig. 4, respectively. In Fig. 3, we can see that the amplitudes of the spectra are relatively large and flat

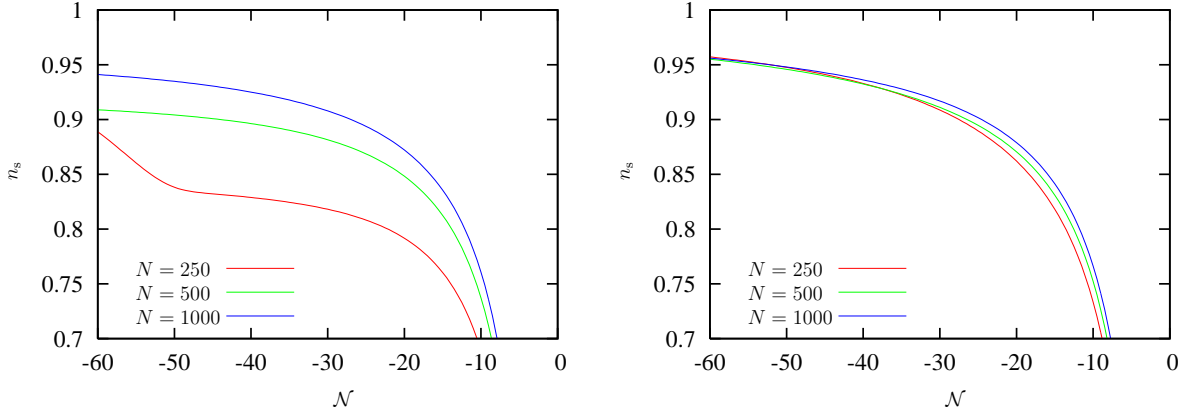


Figure 4: The spectral indices  $n_s$  of the spectra shown in Fig. 3. The shape of the spectrum is identical irrespective of the overall mass scale. In the left panel, the mass distribution follows Eq. (30), with the lightest mass being 1/100 of the heaviest one: for the case of  $N = 250$  where we can obtain  $\mathcal{N} \sim 60$ ,  $n_s$  is decreasing quickly at the early stages due to the “drop-out” effect of the massive fields. For the Marčenko-Pastur law given by Eq. (32) where the masses are much more densely spaced, shown in the right panel, this effect is very weak and  $n_s$  looks more or less the same at 60  $e$ -folds before the end of inflation. Still we can see that the index for  $N = 250$  case is redder than  $n_s$  for  $N = 1000$  case.

compared with the corresponding curves in the upper row where the exponential distribution of the previous section, Eq. (30), is applied. Larger amplitude is easily anticipated from the fact that masses are densely spaced: the most massive field is 100 times heavier than the lightest one in the upper row, while now it is less than 6 times. Hence the energy density is large with the same initial conditions thus correspondingly  $\mathcal{P}$  is also large. Flatter spectrum could be understood in the same way: since the masses are very close to each other, the drop-out effect is weak and hence the spectra with different numbers of fields look very similar. This is clearly seen by the spectral index shown in Fig. 4. Unlike the case of the exponential distribution shown on the left panel,  $n_s$ ’s look very similar now. Still,  $n_s$  for the case of 250 fields is slightly redder than the other cases where more fields support inflation so the effect of the slow-roll is more powerful. We have summarised the results of the current and the previous sections in Table 2.

### 4.3 Comparison with single field case

As we have seen in the previous sections, the number of the axion fields and the corresponding mass distributions have important effects on the power spectrum and the spectral index. And this affects the physical quantities at the end of the inflationary epoch we have calculated in Section 3. To get clearer idea, in this section we compare two mass distributions we have discussed in the previous sections for multi-field inflation with the case of single field inflation.

We have performed numerical calculations on the basis of the single field inflation of Section 2, where we set  $\phi_i = 20m_{\text{Pl}}$  and  $m = 10^{-5}m_{\text{Pl}}$ . We have tried total 400 fields for multi-field case, and for comparison we have set the average mass the same: for the exponential distribu-

tion, Eq. (30),

$$m_1 = 10m_{400} = 2.15313 \times 10^{-5} m_{\text{Pl}}, \quad (34)$$

i.e. the lightest mass is 1/10 of the heaviest mass. We simply set  $\bar{m} = 10^{-5} m_{\text{Pl}}$  for the Marčenko-Pastur law, Eq. (32), then we have

$$\begin{aligned} m_1 &= 1.69594 \times 10^{-5} m_{\text{Pl}}, \\ m_{400} &= 0.299126 \times 10^{-5} m_{\text{Pl}}. \end{aligned} \quad (35)$$

We have set all the initial amplitudes the same,

$$\begin{aligned} \phi_i^{(0)} &= 1.00000 m_{\text{Pl}}, \\ \phi_i^{(0)} &= 0.999968 m_{\text{Pl}} \end{aligned} \quad (36)$$

for the exponential distribution and the Marčenko-Pastur distribution respectively, making the initial Hubble parameters  $H_{\text{ini}}$ 's for all the three cases identical. In Fig. 5 and Table 3, we show the results of the calculations.

In the left panel of Fig. 5, we plot the power spectra  $\mathcal{P}$ . Since  $H_{\text{ini}}$ 's are the same, the amplitude of  $\mathcal{P}$ 's are identical initially. However, as inflation proceeds they drop at different rates:  $\mathcal{P}$  for the single field case is most slowly evolving, while for multi-field cases we obtain steeper spectra. Here, how quickly the spectrum is decreasing depends on the density of the masses: if the mass density is high, i.e. masses of the fields are densely packed, the drop-out effect is alleviated and the spectrum is slowly changing compared with the case of sparse mass density. This is clearly seen in the right panel of Fig. 5 which shows the spectral indices  $n_s$ . Note that at later stage, around  $\mathcal{N} \sim 80$ ,  $n_s$  under the Marčenko-Pastur law becomes steeper than the one under the exponential distribution: following Eq. (30), the masses of the fields are densely placed in the lighter region. Thus at later stages where light fields support inflation the energy density under the exponential distribution is changing more mildly, making the spectrum bluer.

## 5 Conclusions

In this paper we have examined the dynamics of multi-field inflation at its final stage and the density perturbations. Within the slow-roll regime, the fields follow the evolution equations Eq. (17) according to their masses and we can write all the fields and their derivatives in terms of the lightest field as Eq. (19). Then, the Hubble parameter at the end of inflation,  $H_{\text{end}}$ , becomes independent of many factors, e.g. initial values and the number of the fields and the detail of the mass distribution, and is approximated to the lightest mass  $m_N$  only, given by Eq. (21). Also the amplitude of the lightest field at the end of inflation,  $\phi_N^{\text{end}}$ , depends on the number of fields which have not yet relaxed to the minima of the potentials as Eq. (26). The power spectrum  $\mathcal{P}$  and the spectral index  $n_s$  given by Eqs. (28) and (29) respectively, however, cannot be calculated in the same way because many fields other than the lightest one contribute at earlier stages of inflation.

The detail of the mass distribution greatly affects  $\mathcal{P}$  and  $n_s$ : we have investigated the exponential distribution, Eq. (30), and the Marčenko-Pastur law, Eq. (32). It seems that three

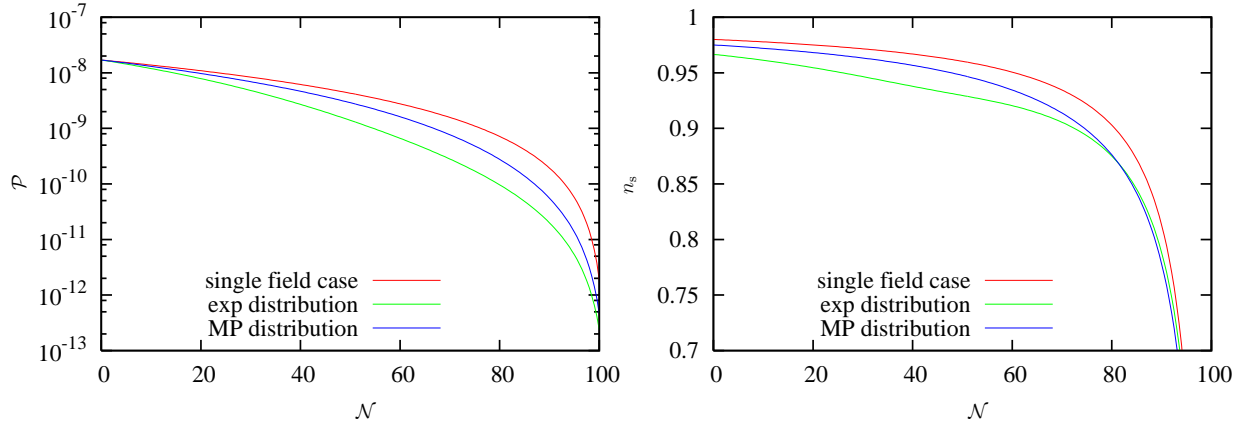


Figure 5: Plots of the power spectra  $\mathcal{P}$  (left panel) and the spectral indices  $n_s$  (right panel). Here we set  $\mathcal{N} = 0$  to be the beginning of the inflationary phase. At  $\mathcal{N} = 0$ , the amplitudes of the power spectra for all the three cases are the same, but the spectral indices are not: this is because for the exponential distribution the masses are sparsely placed in heavy region, so the drop-out effect is larger at early times. Note that since the masses are densely packed in light region for the exponential distribution, more fields support inflation at late stages than for the Marčenko-Pastur distribution and hence  $n_s$  becomes larger before the end of inflation.

factors of the mass distribution, namely, the number of the fields  $N$ , the overall mass scale, and the density of masses in the range over which they are spread. The amplitude of the power spectrum  $\mathcal{P}$  depends on the overall mass scale, and the spectral index  $n_s$  is independent of the mass scale but is affected by the two other factors. The ‘‘drop-out’’ effect is crucial here: the most massive axions fall to their minima at the early stages of inflation and their energies are dissipated by the large Hubble parameter, completely dropping out of the inflationary regime and contribute no more. This leads to the relatively steep decrease in  $H$  and hence makes  $n_s$  redder than the single field case. If the masses are densely packed and the number of the fields are large, the drop-out effect is alleviated because soon the slowly rolling fields dominates the energy density.

Note that, however, detail of the initial conditions and the masses of the axion fields depend on the structure of the microphysics of string compactification. Although it is a formidable task to calculate any specific and concrete realisation from the first principle, this would be an important subject to implement a consistent and successful scenario of inflation in the context of string theory.

## Acknowledgements

I thank Kiwoon Choi, Hongsu Kim and Soo A Kim for useful conversations. Especially I am indebted to Ki-Young Choi and Andrew Liddle for many important correspondences and suggestions. It is also a great pleasure to thank Seung-Hoon Cha, Sungwook Hong, Donghui Jeong and Kwangil Seon for helpful comments on numerical computations.

## References

- [1] See, e.g. A. Linde, *Particle physics and inflationary cosmology*, Harwood Academic Press (1990) ; A. R. Liddle and D. H. Lyth, *Cosmological inflation and large scale structure*, Cambridge University Press (2000)
- [2] U. Seljak et al., *Phys. Rev.* **D 71**, 103515 (2005) [astro-ph/0407372](#) ; J. K. Adelman-McCarthy et al., *Astrophys. J. Suppl.* **162**, 38 (2006) [astro-ph/0507711](#)
- [3] D. N. Spergel et al., [astro-ph/0603449](#)
- [4] S. Kachru, R. Kallosh, A. Linde and S. P. Trivedi, *Phys. Rev.* **D 68**, 046005 (2003) [hep-th/0301240](#)
- [5] See, e.g. A. Linde, [hep-th/0503195](#)
- [6] S. Dimopoulos, S. Kachru, J. McGreevy and J. G. Wacker, [hep-th/0507205](#)
- [7] A. R. Liddle, A. Mazumdar and F. E. Schunck, *Phys. Rev.* **D58**, 061301 (1998) [astro-ph/9804177](#) ; P. Kanti and K. Olive, *Phys. Rev.* **D 60**, 043502 (1999) [hep-ph/9903524](#) ; E. J. Copeland, A. Mazumdar and N. J. Nunes, *Phys. Rev.* **D 60**, 083506 (1999) [astro-ph/9904309](#) ; For a realisation using non-perturbative interaction between branes, see, e.g. K. Becker, M. Becker and A. Krause, *Nucl. Phys.* **B 715**, 349 (2005) [hep-th/0501130](#), and in the context of open string theory, see, e.g. H. Singh, [hep-th/0608032](#)
- [8] R. Easther and L. McAllister, *J. Cosmol. Astropart. Phys.* **05**, 018 (2006) [hep-th/0512102](#)
- [9] S. A. Kim and A. R. Liddle, *Phys. Rev.* **D 74**, 023513 (2006) [astro-ph/0605604](#)
- [10] See, e.g. G. Jungman, M. Kamionkowski and K. Griest, *Phys. Rept.* **267**, 195 (1996) [hep-ph/9506380](#)
- [11] D. H. Lyth, *Phys. Lett.* **B 579**, 239 (2004) [hep-th/0308110](#) ; J.-O. Gong, *Phys. Lett.* **B 637**, 149 (2006) [hep-ph/0602106](#)
- [12] D. H. Lyth and D. Wands, *Phys. Lett.* **B 524**, 5 (2002) [hep-ph/0110002](#) ; T. Moroi and T. Takahashi, *Phys. Lett.* **B 522**, 215 (2002) [hep-ph/0110096](#) *Erratum-ibid.* **B 539**, 303 (2002)
- [13] L. Kofman, A. Linde and A. A. Starobinsky, *Phys. Rev. Lett.* **73**, 3195 (1994) [hep-th/9405187](#) ; L. Kofman, A. Linde and A. A. Starobinsky, *Phys. Rev.* **D 56**, 3258 (1997) [hep-ph/9704452](#)
- [14] J. Ellis, J. E. Kim and D. V. Nanopoulos, *Phys. Lett.* **B 145**, 181 (1984)
- [15] J. Yang, M. S. Turner, G. Steigman, D. N. Schramm and K. A. Olive, *Astrophys. J.* **281**, 493 (1984) ; T. P. Walker, G. Steigman, D. N. Schramm, K. A. Olive and H.-S. Kang, *Astrophys. J.* **376**, 51 (1991) ; S. Sarkar, *Rept. Prog. Phys.* **59**, 1493 (1996) [hep-ph/9602260](#)

- [16] J.-O. Gong, *Class. Quant. Grav.* **21**, 5555 (2004) [gr-qc/0408039](#)
- [17] E. D. Stewart and J.-O. Gong, *Phys. Lett. B* **510**, 1 (2001) [astro-ph/0101225](#) ; J. Choe, J.-O. Gong and E. D. Stewart, *J. Cosmol. Astropart. Phys.* **07**, 012 (2004) [hep-ph/0405155](#)
- [18] A. R. Liddle and S. M. Leach, *Phys. Rev. D* **68**, 103503 (2003) [astro-ph/0305263](#)
- [19] P. Kanti and K. A. Olive, *Phys. Rev. D* **60**, 043502 (1999) [hep-ph/9903524](#) ; P. Kanti and K. A. Olive, *Phys. Lett. B* **464**, 192 (1999) [hep-ph/9906331](#)
- [20] J.-O. Gong, [hep-ph/0610423](#)
- [21] B. A. Bassett, S. Tsujikawa and D. Wands, *Rev. Mod. Phys.* **78**, 537 (2006) [astro-ph/0507632](#)
- [22] A. A. Starobinsky, *JETP Lett.* **42**, 152 (1985) ; M. Sasaki and E. D. Stewart, *Prog. Theor. Phys.* **95**, 71 (1996) [astro-ph/9507001](#) ; M. Sasaki and T. Tanaka, *Prog. Theor. Phys.* **99**, 763 (1998) [gr-qc/9801017](#) ; J.-O. Gong and E. D. Stewart, *Phys. Lett. B* **538**, 213 (2002) [astro-ph/0202098](#)
- [23] Y.-S. Piao, *Phys. Rev. D* **74**, 047302 (2006) [gr-qc/0606034](#)
- [24] A. D. Linde, *Phys. Lett. B* **175**, 395 (1986)

mass distribution	N	m	$\mathcal{N}$		$\phi_N^{\text{end}}$		$H_{\text{end}}$		$\mathcal{P}$	$n_s$
			analytic	numerical	analytic	numerical	analytic	numerical		
exponential distribution	250	$m_{\text{Pl}}$	62.50	64.52	0.31427	0.353184	$0.471405 \times 10^{-2}$	$0.604933 \times 10^{-2}$	$4.82272 \times 10^0$	0.891368
		$m_{\text{Pl}}^{-2}$					$0.471405 \times 10^{-4}$	$0.604933 \times 10^{-4}$	$4.82272 \times 10^{-4}$	
		$m_{\text{Pl}}^{-4}$					$0.471405 \times 10^{-6}$	$0.604933 \times 10^{-6}$	$4.82272 \times 10^{-8}$	
		$m_{\text{Pl}}^{-6}$					$0.471405 \times 10^{-8}$	$0.604933 \times 10^{-8}$	$4.82272 \times 10^{-12}$	
	500	$m_{\text{Pl}}$	125.00	127.13	0.219199	0.271686	$0.471405 \times 10^{-2}$	$0.588379 \times 10^{-2}$	$1.80712 \times 10^{-1}$	0.909015
		$m_{\text{Pl}}^{-2}$					$0.471405 \times 10^{-4}$	$0.588379 \times 10^{-4}$	$1.80712 \times 10^{-5}$	
		$m_{\text{Pl}}^{-4}$					$0.471405 \times 10^{-6}$	$0.588379 \times 10^{-6}$	$1.80712 \times 10^{-9}$	
		$m_{\text{Pl}}^{-6}$					$0.471405 \times 10^{-8}$	$0.588379 \times 10^{-8}$	$1.80712 \times 10^{-13}$	
	1000	$m_{\text{Pl}}$	250.00	252.24	0.15396	0.206531	$0.471405 \times 10^{-2}$	$0.576077 \times 10^{-2}$	$3.71709 \times 10^{-2}$	0.941230
		$m_{\text{Pl}}^{-2}$					$0.471405 \times 10^{-4}$	$0.576077 \times 10^{-4}$	$3.71709 \times 10^{-6}$	
		$m_{\text{Pl}}^{-4}$					$0.471405 \times 10^{-6}$	$0.576077 \times 10^{-6}$	$3.71709 \times 10^{-10}$	
Marčenko-Pastur distribution	250	$m_{\text{Pl}}$	62.50	63.69	0.305888	0.375010	$0.142110 \times 10^0$	$0.196380 \times 10^0$	$5.74883 \times 10^1$	0.957510
		$m_{\text{Pl}}^{-2}$					$0.142110 \times 10^{-2}$	$0.196380 \times 10^{-2}$	$5.74883 \times 10^{-3}$	
		$m_{\text{Pl}}^{-4}$					$0.142110 \times 10^{-4}$	$0.196380 \times 10^{-4}$	$5.74883 \times 10^{-7}$	
		$m_{\text{Pl}}^{-6}$					$0.142110 \times 10^{-6}$	$0.196380 \times 10^{-6}$	$5.74883 \times 10^{-11}$	
	500	$m_{\text{Pl}}$	125.00	126.32	0.222222	0.301697	$0.140584 \times 10^0$	$0.188119 \times 10^0$	$3.82160 \times 10^{-3}$	0.955256
		$m_{\text{Pl}}^{-2}$					$0.140584 \times 10^{-2}$	$0.188119 \times 10^{-2}$	$3.82160 \times 10^{-3}$	
		$m_{\text{Pl}}^{-4}$					$0.140584 \times 10^{-4}$	$0.188119 \times 10^{-4}$	$3.82160 \times 10^{-7}$	
		$m_{\text{Pl}}^{-6}$					$0.140584 \times 10^{-6}$	$0.188119 \times 10^{-6}$	$3.82160 \times 10^{-11}$	
	1000	$m_{\text{Pl}}$	250.00	251.45	0.159364	0.239128	$0.139643 \times 10^0$	$0.182052 \times 10^0$	$2.45069 \times 10^1$	0.956110
		$m_{\text{Pl}}^{-2}$					$0.139643 \times 10^{-2}$	$0.182052 \times 10^{-2}$	$2.45069 \times 10^{-3}$	
		$m_{\text{Pl}}^{-4}$					$0.139643 \times 10^{-4}$	$0.182052 \times 10^{-4}$	$2.45069 \times 10^{-7}$	
		$m_{\text{Pl}}^{-6}$					$0.139643 \times 10^{-6}$	$0.182052 \times 10^{-6}$	$2.45069 \times 10^{-11}$	

Table 2: Summary of the numerical calculations we have performed in Sections 4.1 and 4.2. For analytic estimates, we have used the results derived in Section 3. Note that the mass given here denotes the heaviest mass,  $m_1$ , and the average mass  $\bar{m}$  for the exponential distribution and the Marčenko-Pastur law, respectively. Also,  $\phi_{\text{end}}$  and  $H_{\text{end}}$  are given in term of  $m_{\text{Pl}}$ , and  $\mathcal{P}$  and  $n_s$  are evaluated at 60 e-folds before the end of inflation.

		$\mathcal{N}$	$\phi_{\text{end}}$	$H_{\text{end}}$	$\mathcal{P}$	$n_s$
single field inflation	analytic	100.00	0.942809	$0.471405 \times 10^{-5}$	$5.96853 \times 10^{-9}$	0.966359
	numerical	100.97	1.00934	$0.574670 \times 10^{-5}$		
exponential distribution	analytic	100.00	0.121716	$0.101500 \times 10^{-5}$	$2.47245 \times 10^{-9}$	0.936631
	numerical	101.43	0.225956	$0.124816 \times 10^{-5}$		
Marčenko-Pastur distribution	analytic	99.99	0.175075	$0.141009 \times 10^{-5}$	$4.40243 \times 10^{-9}$	0.955755
	numerical	101.27	0.324082	$0.190495 \times 10^{-5}$		

Table 3: Comparison of several quantities between the single field inflation and multiple field inflation models under the mass distributions, Eqs. (30) and (32). As in Tables 2 and 2, here  $\phi_{\text{end}}$  and  $H_{\text{end}}$  are given in terms of  $m_{\text{Pl}}$ , and  $\mathcal{P}$  and  $n_s$  are calculated before 60  $e$ -folds before the end of inflation. Note that since it is not easy to derive analytic estimates for  $\mathcal{P}$  and  $n_s$  for multi-field cases, we only show their numerical results.